International Journal of Applied Earth Observation and Geoinformation 13 (2011) 236–245

Contents lists available at ScienceDirect

International Journal of Applied Earth Observation and Geoinformation

journal homepage: www.elsevier.com/locate/jag

Normalized algorithm for mapping and dating forest disturbances and regrowth for the United States

Liming He[a,*], Jing M. Chen[a,**], Shaoliang Zhang[b], Gustavo Gomez[c], Yude Pan[d], Kevin McCullough[d], Richard Birdsey[d], Jeffrey G. Masek[e]

[a] Department of Geography and Program in Planning, University of Toronto, 100 St. George St., Room 5047, Toronto, ON M5S 3G3, Canada
[b] China University of Mining and Technology, Jiefang Road South, Xuzhou, Jiangsu 221008, China
[c] Ryerson University, 350 Victoria Street, Toronto, ON M5B 2K3, Canada
[d] Newtown Square Corporate Campus, USDA Forest Service, 11 Campus Blvd, Newtown Square, PA 19073, United States
[e] Biospheric Sciences Branch (Code 614.4), NASA Goddard Space Flight Center, Greenbelt, MD 20771, United States

ARTICLE INFO

Article history:
Received 18 January 2010
Accepted 14 December 2010

Keywords:
Forest disturbance
The continental US
Fire
Logging
Disturbance index
Change detection algorithm

ABSTRACT

Forest disturbances such as harvesting, wildfire and insect infestation are critical ecosystem processes affecting the carbon cycle. Because carbon dynamics are related to time since disturbance, forest stand age that can be used as a surrogate for major clear-cut/fire disturbance information has recently been recognized as an important input to forest carbon cycle models for improving prediction accuracy. In this study, forest disturbances in the USA for the period of ~1990–2000 were mapped using 400+ pairs of re-sampled Landsat TM/ETM scenes in 500m resolution, which were provided by the Landsat Ecosystem Disturbance Adaptive Processing System project. The detected disturbances were then separated into two five-year age groups, facilitated by Forest Inventory and Analysis (FIA) data, which was used to calculate the area of forest regeneration for each county in the USA.

In this study, a disturbance index (DI) was defined as the ratio of the short wave infrared (SWIR, band 5) to near-infrared (NIR, band 4) reflectance. Forest disturbances were identified through the Normalized Difference of Disturbance Index (NDDI) between circa 2000 and 1990, where a positive NDDI means disturbance and a negative NDDI means regrowth. Axis rotation was performed on the plot between DIs of the two matched Landsat scenes in order to reduce any difference of DIs caused by non-disturbance factors. The threshold of NDDI for each TM/ETM pair was determined by analysis of FIA data. Minor disturbances affecting small areas may be omitted due to the coarse resolution of the aggregated Landsat data, but the major stand-clearing disturbances (clear-cut harvest, fire) are captured. The spatial distribution of the detected disturbed areas was validated by Monitoring Trends in Burn Severity fire data in four States of the western USA (Washington, Oregon, Idaho, and California). Results indicate omission errors of 66.9%.

An important application of this remote sensing-based disturbance map is to associate with FIA forest age data for developing a US forest age map. The US forest age map was also combined with the Canadian forest age map to produce a continent-wide forest map, which becomes a remarkable data layer for North America carbon cycle modeling.

1. Introduction

Forest disturbances interrupt the natural succession of forest; they range widely in type, duration, spatial extent, rate, and magnitude (or severity) (Wulder and Franklin, 2007). Quantifying disturbance and recovery of ecosystems by remote sensing has been regarded as critical to improve carbon budget estimates at multiple temporal and spatial scales (Frolking et al., 2009). Types of disturbance that can be detected by remote sensing and their detection accuracies depend on the spatial and temporal resolutions of remote sensed images (Wulder and Franklin, 2007). Different change detection algorithms have been applied to mapping forest disturbance, with the specific data and method of the algorithm depending on the nature of the project or research purposed (Coppin et al., 2004; Lu et al., 2004; Hilker et al., 2009).

* Corresponding author. Tel.: +1 416 978 5070; fax: +1 416 946 3886.
** Corresponding author. Tel.: +1 416 978 7085; fax: +1 416 946 3886.
E-mail addresses: liming.he@gmail.com (L. He), chenj@geog.utoronto.ca (J.M. Chen).

0303-2434/$ – see front matter © 2010 Elsevier B.V. All rights reserved.
doi:10.1016/j.jag.2010.12.003

Recently, the Landsat Ecosystem Disturbance Adaptive Processing System (LEDAPS) project has produced wall-to-wall maps of stand-clearing forest disturbance and regrowth for the North America continent over a decade (1990–2000) (Masek et al., 2008). A Tasseled-Cap-based disturbance index was adopted and modified in the project for disturbance detection (Healey et al., 2005). As an index differencing algorithm, a threshold needs to be determined for each Landsat TM/ETM scene or eco-region, and the determination of the threshold was somewhat subjective (Masek et al., 2008). A suitable threshold is critical to identify the changed areas because generally similar bidirectional reflectance distribution functions (BRDF), seasonal and phenological states between multi-temporal images are required in the implementation of the algorithm (Lu et al., 2004). Available remote sensing images rarely conform to such assumptions (Masek et al., 2008, 2006).

As a result of the approach, sharp edges are sometimes found between image scenes in the LEDAPS forest disturbance mosaic (referred to as "edge effect" hereafter). This edge effect could be caused by several factors, such as the mismatch of data acquisition year and date, phenological disparities (Coppin et al., 2004). Such edge effects indicate the existence of systemic noise in the threshold algorithms used for change detection and should be corrected before map mosaicing. This is similar to the finding by Comber et al. (2004) that detected land cover changes between different years may be highly affected by noise because the surface reflectance of unchanged cover types would change between the two moments of observation. The same issue is encountered and addressed in a different way in this study.

To this end, we attempt to reveal and correct the effect of non-disturbance factors which hinder the change detection, and to map forest disturbance for conterminous United States in 500 m resolution following the LEDAPS project approach. We focus on forest disturbances of 500 m or larger corresponding to the data input. A method to determine the thresholds of disturbance degree for each TM/ETM scene has been developed to reduce the edge effect in mosaic maps by introducing the Forest Inventory and Analysis (FIA) data. The detected disturbances were separated into two five-year ages groups, with the aid of FIA data. We discussed the applicability and limitation of our algorithms in Section 5. The forest stand age is reconciled with the disturbance years and is critical information for use in carbon cycle models (Chen et al., 2003; Luyssaert et al., 2008; Song and Woodcock, 2003). The forest stand age derived from disturbance map in this study can be used to update the US forest stand age map (Pan et al., 2010).

2. Data sets

Forest disturbance in the United States was mapped using 400+ pairs of cloud-free Landsat TM/ETM scenes, which were downloaded from the LEDAPS website and have been re-sampled into 500 m resolution (Masek et al., 2006, 2008). Small forest disturbances that could be detected at the original 30 m resolution can be totally missed in the 500 m resolution images. This dataset is centered on 1990 and 2000 epochs, but the actual image acquisition dates vary depending on data availability. Most acquisition dates are from 1986 to 1992 for the 1990-epoch coverage, and 1999 to 2001 for the 2000-epoch coverage. Not all images were acquired during peak-greenness conditions, and the 1990 and 2000 epoch data pairs were not acquired during the same month (Masek et al., 2008; Tucker et al., 2004). This inconsistency in acquisition dates in the year for the two epochs is the primary error source for forest disturbance mapping when various disturbance indexes are used (as shown in Section 3).

The Monitoring Trends in Burn Severity (MTBS) data are used as reference data to assess the accuracy of forest disturbance maps

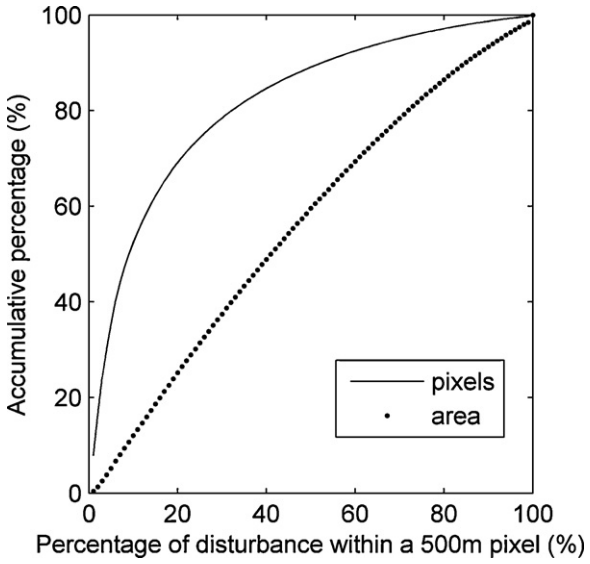

Fig. 1. Cumulative percentages of forest disturbance pixels and area for LEDAPS 500 m product.

(http://mtbs.gov/index.html). The MTBS project is designed to consistently map the burn severity and perimeters of fires across all lands of the United States for the period from 1984 to 2010. The original MTBS product is mapped at 30 m resolution using the differenced Normalized Burn Ratio (dNBR) (Key and Benson, 2005) and includes all fires greater than 2 km^2 in eastern United States (east of longitude 97°W) and greater than 4 km^2 for the rest of the country. The data in four states in western United States (California, Idaho, Oregon, and Washington) between 1987 and 2001, which are composed of 1405 fire events, were selected in this study. Only whole fires or parts of fires occurring in forested land were included in the analysis. These data were re-sampled to 500 m resolution, rendering a reference map. We selected the four western states because of their large disturbed areas that are detectable with the 500 m resolution images.

The FIA program reports on national status and trends in tree growth, mortality, removal by harvest, forest area, and associated human activities (Forest Inventory and Analysis, 2005). Yearly areas of naturally regenerated and managed plantation stands were compiled from the FIA database using 2000 as the baseline year. These data are classified by stand-age and grouped by county. For stand-age 1–10 years, sample plots are classified in one-year increments. These data are used to determine the thresholds in our change detection algorithm and separate the recent 10-year forest disturbances into two five-year regeneration age groups.

Forest cover is an essential input for mapping forest type and forest biomass (Blackard et al., 2008; Ruefenacht et al., 2008) and forest/non-forest masks can be made from MODIS products (Justice et al., 2002), such as percent tree cover (Hansen et al., 2003a,b, 2002). We use the forest cover mask from the US Forest Service (USFS) (Ruefenacht et al., 2008). Water pixels are sometimes shown in the forest cover map due to error in geo-referencing and mixture of pixels in the coarsened TM/ETM images.

The LEDAPS disturbance map in 500 m resolution is used for comparison (Masek et al., 2008). The product includes percentages of disturbed forest area for each 500 m grid over continental North America. The percentages vary from 1 to 100 in steps of 1%. In total, there are ~6.2 million grid cells with disturbance area varying from 1 to 100%. Fig. 1 shows the cumulative percentages of forest disturbance pixels and the areas based on the disturbance level (% disturbed area) in 500 m grids. For example, the number of grids that contain disturbance percentage less than or equal to

20%, is ~4.3 million, which count for 69.1% of total disturbed grids (Fig. 1); however, the corresponded disturbance area of these grids is 7.4 million ha, only count for 25.1% of total disturbed area. This figure implies that it is possible to capture most area of the forest disturbance in 500 m resolution even though smaller disturbance events are missed because bigger disturbance events are easier to be detected and they occupy most of the disturbed area.

3. Mapping and dating forest disturbance

The method of detecting forest disturbance in this study may be considered a Bi-temporal change detection algorithm (Coppin et al., 2004): disturbance index (DI) is used as a differential index and for indicating forest status; then the difference in DIs between two times indicates the change of forest status. The DI can be formed from one or more spectral bands of remote sensing, and has variants in name dependent on the study subject, such as Normalized Burn Ratio (NBR) (Key and Benson, 2005; Roy et al., 2006; Wimberly and Reilly, 2007), Normalized Difference Water Index (NDWI) (Chen et al., 2005; Gao, 1996; Gu et al., 2007). The principle of these indexes is to identify the vegetation water content by combining a short wave infrared (SWIR) band with a near infrared (NIR) band.

The DI used in this study is defined as the ratio of SWIR (band 5) to NIR (band 4) reflectances (Amiro and Chen, 2003). The changes in forest status are represented by the Difference of Disturbance Index (DDI) between circa 2000 and 1990, where the positive DDI means disturbance and the negative DDI means regrowth.

3.1. The non-disturbance factor in DI and its correction

The DDI values of forest pixels can be altered by non-disturbance factors, such as seasonal change, BRDF, as shown in Fig. 2. The *x*-axis and *y*-axis show DI values of forest pixels, in two years respectively, for four different TM/ETM scenes, as indicated by paths and rows in Fig. 2(a)–(d). Fig. 2(a) shows that regrowth and disturbance are symmetrical to the dash line (1:1 line), which indicates *x* equals *y*. Fig. 2(b) shows most DDIs are greater than zero, and Fig. 2(c) shows the opposite. Some water pixels, which cannot be fully masked by the forest map, show stable and higher DIs. Their DIs are close to 1 and DDIs are close to zero, as indicated by the circles in Fig. 2(a) and (b). Fig. 2(d) shows there are more positive DDIs than negative DDIs; burn scars are observed in this ETM scene, and most pixels are close to an obvious axis (refer to the main axis), slightly departing and above the dash line. Pixels close to this axis are not disturbed.

The distribution of pixels in Fig. 2(a)–(d) is generalized in Fig. 2(e). Most pixels are within a triangle outlined by points C, A, and D. The undisturbed pixels are closer to line AB, and the pixels with disturbance or regrowth departs from line AB. The slope of line AB is generally not equal to one. The point A indicates dark dense forest (DDF) pixels with little or no disturbance, where there are both strongest reflectance in NIR and strongest absorption in SWIR. Along the line AB from A to B, a gradual transition occurs from DDF to young forest or partially forested pixels. The absorption in SWIR and the reflection in NIR are both weaker for pixels closer to point B. The spread of scatter plots increases gradually from A to B. This increase implies that the pixels with bigger DI tend to vary more with disturbance or regrowth. The reason is not entirely clear to us, but the pixels in the spread near B are likely within transition zones from forest to other land covers, such as grassland or cropland, whose DI values may be easily affected by seasonal changes or weather related events. The shape of the distribution depends highly on ecosystem, season, BRDF, etc. A spindle or comet shape is common and the core axis (main axis, line AB) is generally obvious among most pairs of images. The position of vertex A is the minimum DI around 0.5–0.6, influenced by a range of factors. If the minimum DI for a specific TM/ETM scene is greater than 0.6, the forest is not in its mature stage of regrowth or the pixels are not pure forest.

Obvious seasonal changes in TM/ETM data pairs can cause departure of the main axis from the 1:1 line, as shown in Fig. 2. The DDF maintains a stable greenness during most of the growing season while the sparse forest is susceptible to various non-disturbance change factors. If these non-disturbance change factors are uncorrected in mapping forest disturbance, either pixels near the point A or point B in Fig. 2 can be overestimated using the original DDI.

To spectrally match each pair of Landsat scenes for accurate quantification of DDI, axis rotation is performed on the plot between DI of the two matched scenes. For each TM/ETM pair, vertex A, representing the limit of *DI*, is first identified with its coordinate (*DIx*, *DIy*), according to the enveloping lines (along lines AC and AD in Fig. 2(e)). For scene pairs whose enveloping lines are not clear, vertex A is defined with its coordinate closer to (0.5, 0.5). Another point is defined as long as it is within the axis AB so that the slope of AB can be calculated. The rotated DIs are computed as:

$$\begin{aligned} DI1990' &= (DI1990 - DIx) \times \cos(r) + (DI2000 - DIy) \times \sin(r) \\ DI2000' &= -(DI1990 - DIx) \times \sin(r) + (DI2000 - DIy) \times \cos(r) \end{aligned} \quad (1)$$

where, *DI*1990 and *DI*2000 are the original DI values in 1990 and 2000, *DI*1990′ and *DI*2000′ are the rotated DIs in 1990 and 2000, and *r* is the slope of line AB expressed in radians. This rotation is demonstrated in Fig. 2(e) and (f): the origin of coordinate is shifted to (*DIx*, *DIy*); then all points are rotated in clockwise direction by an angle *r*, so the main axis will be coincided with *X* axis after rotation. After the rotation, *DI*1990′ is actually its relative *DI* value in 1990, and *DI*2000′ is the increase or decrease (difference) of DI from 1990 to 2000.

It follows from Fig. 2(f) that we assume that the pixels along line A′B′ are undisturbed and pixels on lines A′e or A′f have the same disturbance intensity. A normalized DDI (referred to NDDI) is defined as:

$$\mathrm{NDDI} = \frac{DI2000'}{DI1990'} \quad (2)$$

In this way, any DDI caused by non-disturbance factors, such as seasonal change, BRDF, are expected to be reduced. This triangulation and axis rotation method may be regarded as a form of normalization, and it allows a larger range of variation of DDI points to be disturbed around B′ before disturbances are identified as they are more easily confounded by non-forest disturbance factors.

3.2. Determination of thresholds and dating of forest disturbance using the constraint of FIA data

The temporal change of forest area is often related to different forest management practices, including afforestation (the permanent change in land cover from non-forest to forest), deforestation (forest changed to non-forest), and regeneration from previous disturbances which have led to forest mortality. Following the assumptions that the disturbed areas regenerate in the second year and the fact that the regenerations occurs in the afforested and disturbed forests, the regeneration statistics from FIA data for the specific periods of time are linked to the remotely sensed forest pixels:

$$\sum_{i=1990}^{2000} R_i = f \cdot (A + D) + \delta \quad (3)$$

where R_i is the regeneration area (km^2) in the *i*th year from the FIA statistics; *A* and *D* are total afforested and disturbed areas within the same period, which are the product of the number of pixels (to

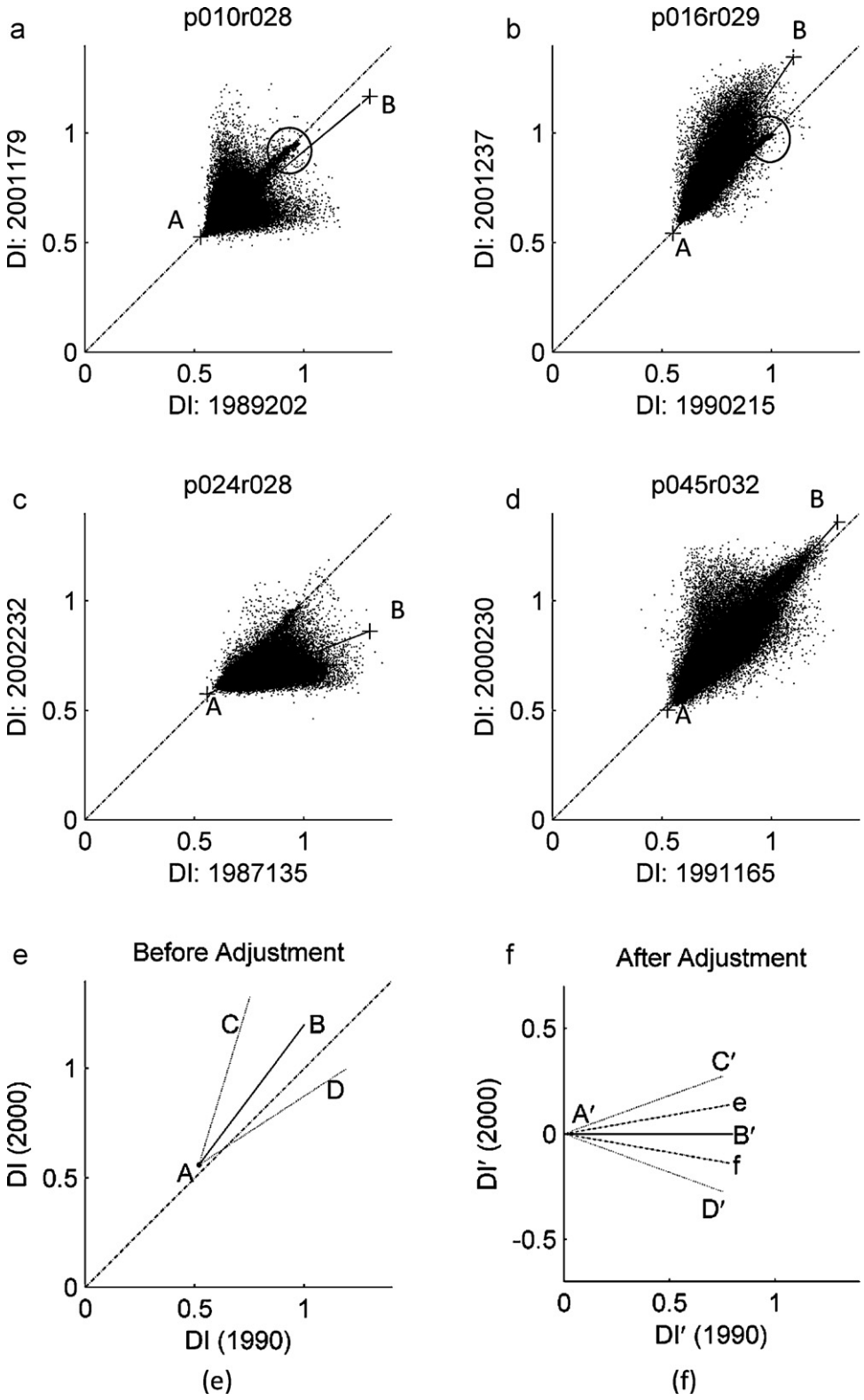

Fig. 2. Demonstration of effect of non-disturbance factors within the DIs and the adjustment.

be determined) and the area of a pixel ($1/4\,km^2$); f is a scale factor related to the sub-pixel fraction of afforestation or disturbance; and δ is the error. The afforestation area, A, is difficult to acquire from the 500 m TM/ETM data, and generally only constitutes a small proportion compared with the forest disturbances, so it is neglected in this study.

The value of the scale factor f depends on the disturbance types (for example, the patch size and the possibility of detection after five or more years) and the resolution of remote sensing data. It is shown from Fig. 1 that many forest disturbance events are at a sub-pixel scale within 500 m grid so f should be less than 1 to let more pixels be taken from the NDDI map. From statistics in LEDAPS 500 m

data (Section 2), f is ~0.19 (29.5 million ha/6.2 million grids/25 ha). It is already known that large omission errors exist if TM/ETM pairs in the 10-year interval are used in detecting forest disturbance. So if 0.19 is used, significant commission errors would be introduced. To avoid excessive commission errors, f is fixed to one in this study. In this way, the total detected disturbed areas in each county are forced to agree with FIA statistics of regeneration data. This also means that remaining commission errors from the detected pixels with partial disturbance are compensated by omission errors from much smaller disturbed areas in these selected pixels. Our final product would therefore capture the large disturbed patches and ensure the integrity of FIA statistics at the county level, even though the sub-pixel disturbance information is lost. As a result, this product is primarily useful for regional applications, such as carbon and water cycle modeling, having the advantage of moderate resolution without involving the complexity of subpixel information.

Based on the fact that the NDDI is generally higher for newly disturbed areas, the NDDI values of all disturbed pixels with $DI2000'$ values greater than 0.02 within each county were sorted in descending order. Then an amount of pixels, N, determined by Eq. (3), is chosen. The threshold NDDI value that produces N is then found for each county. These N pixels were separated into the two five-year age groups, 1990–1995 and 1996–2000, according to the NDDI values and the corresponding areas of the first and second five-year age groups from the FIA statistics. A small threshold of $DI2000'$ (0.02) to detect disturbance areas is selected to avoid pixels around vertex A′ (in Fig. 2(f)) because NDDI values around A′ are very sensitive to errors caused by selection of points A and B in Fig. 2(e).

The dating of forest disturbance can be influenced by the spatial resolution of remotely sensed data and the omission errors in the product in two ways: (1) the NDDI value of new forest disturbance in the sub-pixel scale can be diminished by the background so it cannot be differentiated from the forest disturbance with low NDDI in highly covered forest pixels. This would result in overestimation of disturbance age for forests smaller than a full pixel. (2) We matched the reliable FIA regeneration area to the pixel area in the algorithm ($f = 1$) in order to avoid introducing commission errors in the result. So FIA regeneration areas over 10 years are represented by these forest disturbances which can be easily detected in the later part of 1990s by remote sensing. This approach will also result in overestimation of forest disturbance age.

3.3. Application of the algorithm to the continental U.S.

The general processing steps for each TM/ETM scene (or each county) are described in Fig. 3. First, $DI1990$ and $DI2000$ are derived from a TM/ETM pair for the forest pixel using the forest/non-forest mask. Second, point A and the slope of line AB (in Fig. 2(e)) are determined from their scatter plot. Third, the NDDI are derived as described in Section 3.1. Fourth, the threshold for the NDDI is determined according to the FIA data (Section 3.2), and the forest disturbance pixels are obtained. Finally, the forest disturbance pixels are separated into two age-groups. Then all the disturbance maps for each county are mosaiked to produce a conterminous U.S. map. The point A and slope of line AB are determined semi-automatically (Fig. 2) and all other processing steps are made using Matlab software from MathWorks, Inc. The point A is first selected manually from a scattering plot then the slope of line AB is determined by regression (least square method). The determination of position of line AB may be slightly influenced by the choice of A and the regressed line AB needs inspection to ensure it is not affected by a small group of pixels with extreme values.

Three ways were also used to further reduce the errors which can be introduced by non-disturbance factors:

(1) TM/ETM scenes that have the same acquisition date in 1990 and also same acquisition date in 2000 (the two dates may be different) are grouped together first. A total of 128 TM/ETM pairs were found in 58 groups (each group has several TM/ETM pairs, with all TM scenes in the same date, and all ETM scenes in the same date). The pixels within the same group are put together to determine point A and the slope. Adjacent pairs within the same group are directly mosaiked to a patch, in order to increase the possibility that a county is entirely covered by an image.
(2) Counties fully covered within the same TM/ETM pairs or patches are processed first. A total of 2392 counties satisfied this condition. Most of these counties are in eastern and middle United States, and their areas are relative small compared with western counties.

    The yearly regeneration areas from the FIA statistics for all counties within the same pair of images, or patches, are summed up and used to determine the threshold of NDDI (step 4). FIA data representing regeneration before 1990 are not used for the determination. We did not include these areas because the focus of this study is to detect recently disturbed areas between 1990 and 2000. We determined a threshold for each image pair but not county by county because this approach would reduce the errors of mismatching with FIA data which could be directly passed to the algorithm. In this way, the determined disturbance area for each county does not have to be exactly equal to the county's regeneration area from FIA statistics.
(3) For the remaining 843 counties included in FIA statistics, a mosaic processing is done before the disturbance pixels are determined. For each county, the processing step 4 shown in Fig. 3 is followed separately for each TM/ETM pair within a county boundary. The scene that contains the largest area of this county is used as the master image and all its pixels are kept; then the remaining scenes, as minor images, are merged into the master image in descending order of the areas of the county they contained, until the whole county is within the mosaic patch. This approach is used to minimize the NDDI's difference between adjacent pairs with different acquisition dates.

After these processing steps, the results for all counties are mosaiked, and a forest age map of recent forest disturbance is produced for conterminous USA (Fig. 4). The acquisition dates of TM/ETM pairs are also recorded during the processing.

4. Results and validation

The quality of the forest disturbance mapping was assessed through both visual examination and quantitative analysis against an independent dataset. The disappearance of the edge effect in the mosaiked map indicates the effectiveness of our algorithm in providing consistent results among counties (Fig. 5). Panels a1, b1, c1 and d1 in Fig. 5 shows LEDAPS forest disturbance percentage maps at 500 m resolution, and panels a2, b2, c2 and d2 in Fig. 5 shows our disturbance age maps of the same areas, respectively. The imprints of TM/ETM frames (light blue lines) in the LEDAPS maps indicate that their algorithm is susceptible to the differences among image pairs. These artifacts are greatly reduced in our product. Minor edge effects can still be observed at some county boundaries if those counties have relatively large or small areas of forest regeneration from the FIA statistics, compared with their adjacent counties. For example, a county with blank area implies there is no FIA data or no disturbance.

A single fire event in the MTBS data generally occurred in the same year. From checking the disturbance age map, some burn scars are entirely classified into the same age groups, while oth-

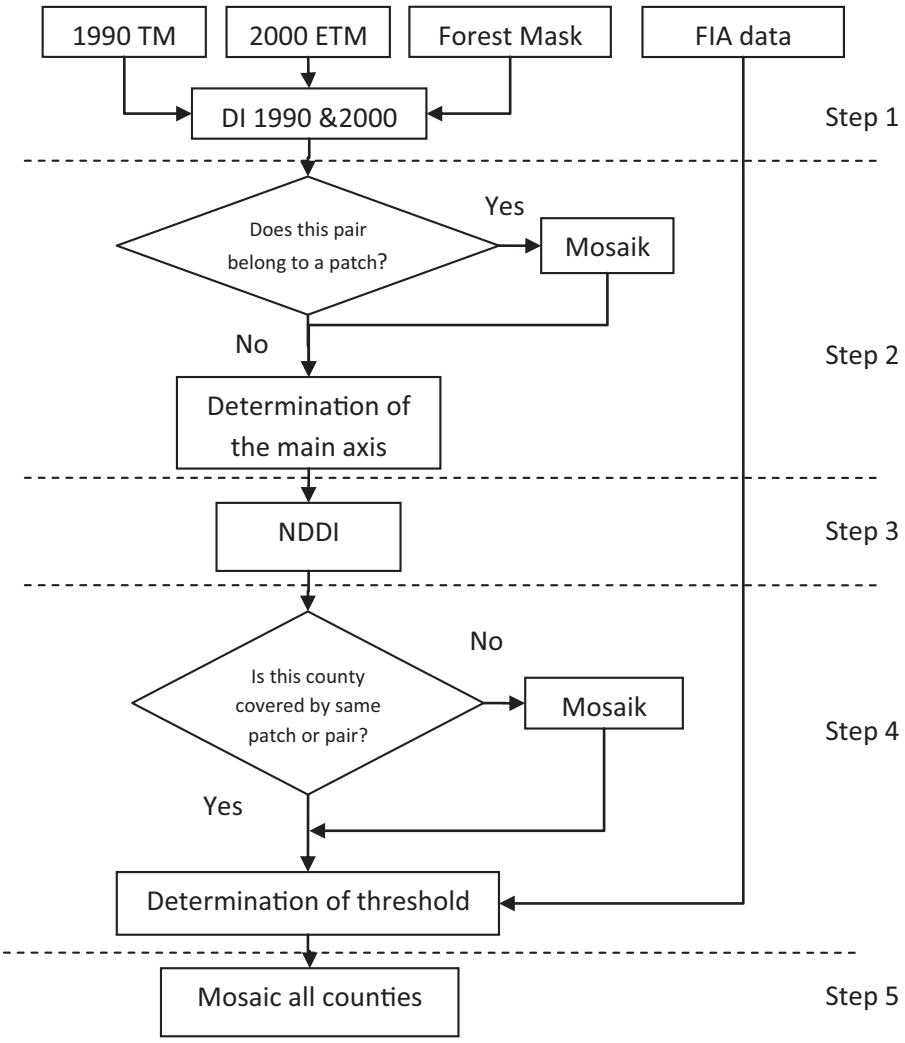

Fig. 3. Flow chart illustrating the forest disturbance mapping method.

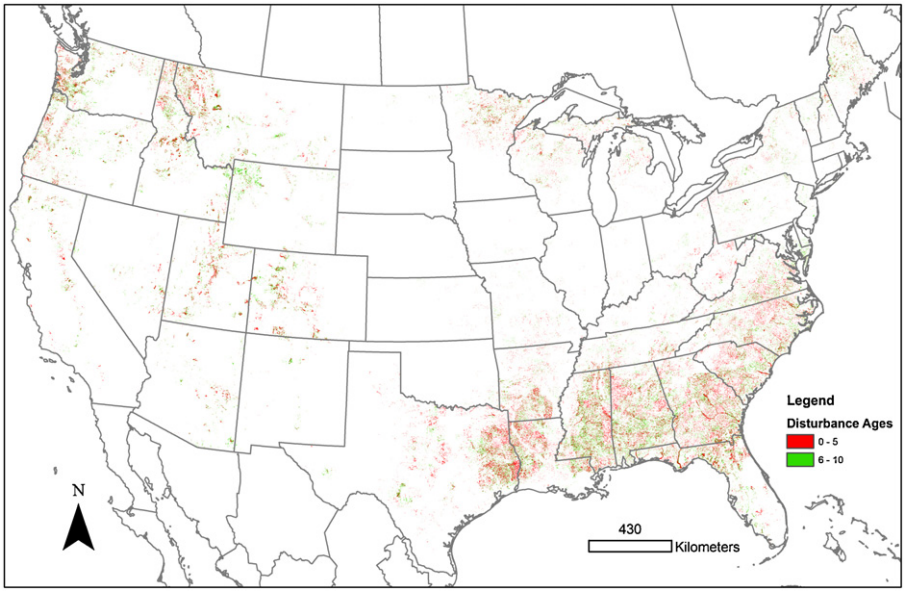

Fig. 4. Forest disturbance age map in two age-groups from 1990 epoch to 2000 epoch.

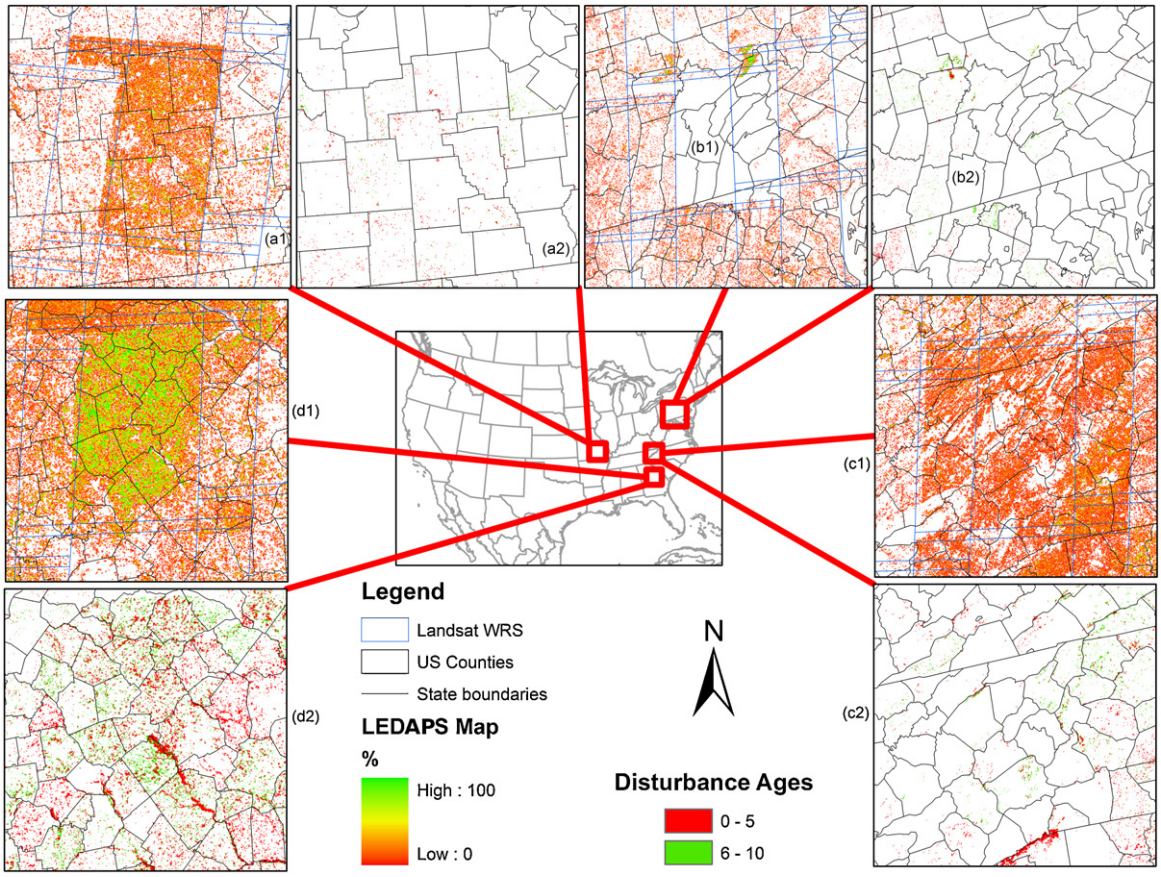

Fig. 5. Comparison of the LEDAPS forest disturbance (panel a1, b1, c1, and d1) product with ours (panel a2, b2, c2, and d2).

ers are divided into two age groups, with the central part of a burn scar classified in the 0–5-year age group, and the fringe areas in the 6–10-year age group. This indicates that our algorithm is effective in detecting recent forest disturbance but the dating accuracy may be inaccurate. The error in dating fire scars may be caused by errors in omitting small disturbed areas due to the coarse spatial resolution of the images. Some counties have FIA regeneration areas mainly in the first or the last five-year age groups, and the dominating red or green color within these counties shown in Fig. 5 (d2) reflects that the use of FIA statistics as the additional control is very important in dating the disturbance.

An error matrix can be produced if an entire forest disturbance map in the testing area exists, so both commission and omission errors can be quantified (Lu et al., 2004). However, the limited availability of reference disturbance data, MTBS burn scar maps, only enable us to validate the omission errors of our algorithm in detecting burn scars. It was found that there are 282,245 disturbed pixels in the 500 m LEDAPS map for the four western US states, and 87,553 disturbed pixels in our map. There were 52 counties with zero regeneration area in FIA data, out of 162 counties in these four states. It was found that 22 counties in the LEDAPS product, or 23 counties in our product, had MTBS burn scar areas larger than zero and also zero FIA regeneration area, within the four states. The thresholds are forced to zero for 16 out of the 23 counties in our product due to the constraint of FIA data, so omission errors are caused by such a constraint. The LEDAPS algorithm detected 19,255 burned pixels, out of the whole 53,089 burned pixels in the reference map (an omission error of 63.7%), while our algorithm detected 16,241 burned pixels, out of the whole 50,833 burned pixels (an omission error of 68.1%) for all the 162 counties. In contrast, LEDAPS algorithm detected 18,933 burned pixels, out of 51,286 burned pixels in the reference map (an omission error of 63.1%), and our algorithm detected 16,216 burned pixels, out of the 48,949 burned pixels (an omission error of 66.9%) for the 110 counties with FIA regeneration area larger than zero. The numbers of burned pixels in these two reference maps are different because the mosaicked disturbance maps used for two algorithms have different overlap areas of the adjacent TM/ETM scenes. The omission error of our algorithm is slightly higher than that of the LEDAPS algorithm (~4%), but the result is still encouraging for two reasons: (1) since our detection is processed at 500 m resolution, it is understandable that partially burned pixels can be missed when using such middle-resolution images; (2) our algorithm uses only 30% of the LEDAPS disturbance pixels to achieve almost the same level of omission errors as LEDAPS.

The regeneration area within the 10-year interval (1990–2000) from the four states' FIA statistics is 2.06×10^4 km^2. The disturbed area in the LEDAPS product for the four states is 1.20×10^4 km^2 (taking account of the percentage of disturbance area in each pixel). Our algorithm reports a disturbance area of 2.19×10^4 km^2, as we set up the scaling factor = 1 for the pixels with FIA regenerated areas.

The regeneration area in FIA statistics for the conterminous United States in 1990s is 2.28×10^5 km^2. The forest disturbance area detected by 500 m LEDAPS product is 1.30×10^5 km^2 (sum up all the percentages $\times$ 0.01 $\times$ 0.25 km^2), which is different from the area reported by previous LEDAPS product (21.7 million ha). The disturbance area in our product is 1.81×10^5 km^2. This area is close to but still less than the FIA statistics. It is understandable that this area is less than the FIA statistics because some image acquisition dates are later than 1990 for the 1990 epoch, or earlier than 2000 for the 2000 epoch, which missed disturbance information in the time gaps.

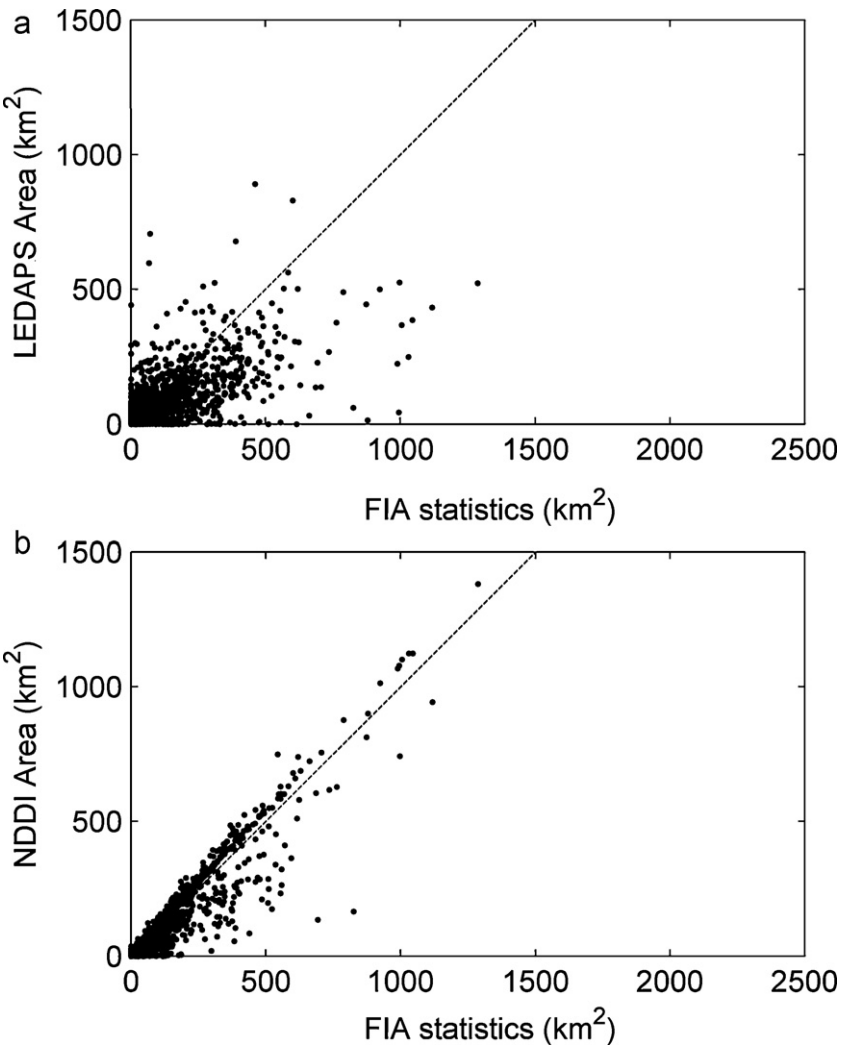

Fig. 6. Comparison of county-level forest regeneration area in 1990s from the FIA statistics with the disturbance area from LEDAPS and our product.

Fig. 6(a) shows the scatter plot of county-level 10-year regeneration areas from FIA statistics vs. corresponding forest disturbance areas from the LEDAPS product. Fig. 6(b) shows the comparison between FIA statistics and forest disturbance areas from our product. The scatter in Fig. 6(b) is much closer to the 1:1 line than that in Fig. 6(a), demonstrating the improvement made by using the FIA data in disturbance mapping and also showing that the county-level forest disturbance statistics are reasonably well represented by our product. 89 counties are excluded from Fig. 6 due to obvious mismatch between remote sensed data and FIA data.

5. Discussion

We have demonstrated that non-disturbance factors can hinder the disturbance detection using satellite images acquired at two different dates. The triangulation and axis rotation techniques for DI normalization are some of the ways to minimize the influence of such non-disturbance factors. The forest in southern US can recover from last disturbance very quickly within 10 years. We have realized that such disturbance can only be accurately observed from TM/ETM data in shorter intervals (Masek et al., 2008), and our results for southern USA can be much improved when more frequent data are used. However, the techniques developed in this study would pave the way for such large volume data processing for disturbance detection.

It should be pointed out in Fig. 6 that the results from NDDI are constrained using the FIA data so the dots in scatter plot are forced to match the 1:1 line. This constrain is one of ways to determine the threshold of NDDI to map disturbance, and it may also propagate any errors in the FIA data itself, which may still be considerable at the county level because of the representativeness of sampling plots. To reduce the possible county-level bias errors, we have used the total areas from all the counties within same TM/ETM pair or patch, where possible, to determine one threshold for this pair/patch. Because the degree of reflectance change in undisturbed areas between two dates can vary spatially for a variety of reasons, the FIA data are the best available nation-wide dataset for individually determining the threshold for every image pair.

Our method is designed for detecting major forest disturbances for use in regional carbon cycle modeling. It would be questionable to assign forest ages to mixed pixels or pixels containing partial disturbance (e.g., thinning). In Eq. (3), f is set to 1 in this study. Its value is used to match the regeneration area from FIA data and the real disturbance area within mixed pixels. As we have discussed in Section 3.2, its value is highly dependent on the disturbance type and the image spatial resolution. When the disturbed area is larger than a pixel, it is reasonable to set f to 1. However when subpixel disturbance occurs, it must be set to values less than 1 in order to capture the disturbance. However, in this way "appar-

ent" commission errors are introduced. For fast recovery forest, f also should be given relatively large values as the detectable disturbance area would otherwise be less than the FIA area. When high resolution and short interval data are used to map disturbance, f should obviously be set to 1.

In short, our algorithm is most applicable to the conditions that (1) the disturbance extent is larger than the pixel size; (2) the disturbance is still detectable from the data from two temporal phases; and (3) FIA data are available. In fact, the first two conditions are always required in any disturbance detection algorithms, and these two conditions can be satisfied as long as short interval and high resolution data (such as TM, ETM, and ASTER) are available. When FIA data are unavailable, the LEDAPS approach to determine thresholds is still applicable to our algorithm.

This study is based on the 500 m data from the LEDAPS project when the TM and ETM data were not free. Now it is feasible to map the forest disturbance in shorter intervals at less cost. The disturbance map for the 1990s is still useful in updating the forest age map in US (Pan et al., 2010), because forest age is generally accepted as a primary driver of forest structure and function, and many components of the forest carbon cycle are related to forest age (Bradford et al., 2008).

6. Concluding remarks

This study demonstrated the capability of moderate resolution remotely sensed data for mapping and dating forest disturbance at the continental scale. A change detection algorithm for detecting forest disturbance was developed and tested using Landsat TM/ETM data aggregated to 500 m resolution. The algorithm uses disturbance index (DI), the ratio of short-wave infrared (band 5) to near-infrared (band 4) reflectances of TM/ETM, as an indicator of forest status, and the Normalized Difference in DI (NDDI) between two dates as a means to detect changes in forest status. Image pairs acquired around 1990 and 2000 were used for disturbance detection. Several techniques were developed to reduce the noise in the detected disturbance map caused by non-forest disturbance factors, including seasonal variations and gradual forest density changes between 1990 and 2000 images. The DI values for the 1990 epoch and 2000 epoch are normalized against each other to reduce the effects on the variations through rotating the main regression line through their scattering plot. The normalization and adjustment of original DIs for reducing the impact of non-disturbance factors enables the algorithm to detect changes caused by real disturbances. The separations of all forest disturbances into two age-groups are also made through using the FIA annual forest stand age statistics at the county level. A forest disturbance map of the conterminous United States in the period from 1990 to 2000 is therefore produced.

The forest disturbance map was evaluated through both visual examination and comparison against MTBS reference data. Compared with the existing LEDAPS product, our disturbance product made two improvements: (1) artifacts shown as distinct boundaries on the Landsat image mosaics were greatly reduced using our DI normalization procedure (Fig. 5); and (2) the disturbance statistics at the county level were brought to close agreement with FIA statistics after they were used for setting thresholds in the disturbance detection. However, our algorithm has a greater omission error than the LEDAPS product (66.9% vs. 63.1%) due to the coarse resolution of the images used. In spite of this limitation, our algorithm can still capture most of the area of forest disturbances at the county level. This disturbance product has been used for improving a FIA-data based forest age map (Pan et al., 2010) and can used for carbon cycle studies at continental and regional scales. Similar to the LEDAPS project, our result also suggests that the omission errors can only be reduced by introducing data in shorter intervals.

Despite discernible improvements, our product cannot provide the exact percentage of forest disturbance in each pixel due to the limitation of the image resolution. The determination of the main regression line in a scatter plot of an image pair needed in our DI normalization algorithm may be influenced to some extent by subjectivity. In the future, the product quality is expected to be further improved by developing an automatic method to determine the regression line and by using high resolution data with short repeat intervals. This study provides a benchmark for continent-wide disturbance mapping using moderate resolution remote sensing imagery. Our disturbance mapping methodology can be further used with high-resolution images to improve mapping small disturbance areas.

Acknowledgements

The authors are grateful to Dr. John Holm and Dr. Ziliang Zhu for their support in this project. We thank Jeffrey G. Masek for providing the Landsat TM/ETM data in 500 m resolution and LEDAPS product. We also thank the US forest service for funding to conduct this research. The authors thank the two anonymous reviewers for their valuable suggestions on the manuscript.

References

Amiro, B.D., Chen, J.M., 2003. Forest-fire-scar aging using SPOT-VEGETATION for Canadian ecoregions. Canadian Journal of Forest Research 33, 1116–1125.

Blackard, J.A., Finco, M.V., Helmer, E.H., Holden, G.R., Hoppus, M.L., Jacobs, D.M., Lister, A.J., Moisen, G.G., Nelson, M.D., Riemann, R., Ruefenacht, B., Salajanu, D., Weyermann, D.L., Winterberger, K.C., Brandeis, T.J., Czaplewski, R.L., McRoberts, R.E., Patterson, P.L., Tymcio, R.P., 2008. Mapping U.S. forest biomass using nationwide forest inventory data and moderate resolution information. Remote Sensing of Environment 112, 1658–1677.

Bradford, J.B., Birdsey, R.A., et al., 2008. Tree age, disturbance history, and carbon stocks and fluxes in subalpine Rocky Mountain forests. Global Change Biology 14, 2882–2897.

Chen, J.M., Ju, W., Cihlar, J., Price, D., Liu, J., Chen, W., Pan, J., Black, A., Barr, A., 2003. Spatial distribution of carbon sources and sinks in Canadas forests. Tellus B 55, 622–641.

Chen, D., Huang, J., Jackson, T.J., 2005. Vegetation water content estimation for corn and soybeans using spectral indices derived from MODIS near- and short-wave infrared bands. Remote Sensing of Environment 98, 225–236.

Comber, A., Fisher, P., et al., 2004. Integrating land-cover data with different ontologies: identifying change from inconsistency. International Journal of Geographical Information Science 18 (7), 691–708.

Coppin, P, Jonckheere, I., Nackaerts, K., Muys, B., Lambin, E., 2004. Digital change detection methods in ecosystem monitoring: a review. International Journal of Remote Sensing 25, 1565–1596.

Forest Inventory and Analysis, 2005. Forest Inventory and Analysis National Core Field Guide, volume 1: Field Data Collection Procedures for Phase 2 Plots, version 3.0. U.S. Department of Agriculture Forest Inventory and Analysis, Washington, DC, p. 203.

Frolking, S., Palace, M.W., Clark, D.B., Chambers, J.Q., Shugart, H.H., Hurtt, G.C., 2009. Forest disturbance and recovery: a general review in the context of spaceborne remote sensing of impacts on aboveground biomass and canopy structure. Journal of Geophysical Research-Biogeosciences, 114.

Gao, B.-c., 1996. NDWI—a normalized difference water index for remote sensing of vegetation liquid water from space. Remote Sensing of Environment 58, 257–266.

Gu, Y.X., Brown, J.F., Verdin, J.P., Wardlow, B., 2007. A five-year analysis of MODIS NDVI and NDWI for grassland drought assessment over the central Great Plains of the United States. Geophysical Research Letters, 34.

Hansen, M.C., DeFries, R.S., Townshend, J.R.G., Sohlberg, R., Dimiceli, C., Carroll, M., 2002. Towards an operational MODIS continuous field of percent tree cover algorithm: examples using AVHRR and MODIS data. Remote Sensing of Environment 83, 303–319.

Hansen, M.C., DeFries, R.S., Townshend, J.R.G., Carroll, M., Dimiceli, C., Sohlberg, R.A., 2003a. Development of 500 meter vegetation continuous field maps using MODIS data. In: Igarss 2003: IEEE International Geoscience and Remote Sensing Symposium, vols. I–VII, Proceedings , pp. 264–266.

Hansen, M.C., DeFries, R.S., Townshend, J.R.G., Carroll, M., Dimiceli, C., Sohlberg, R.A., 2003b. Global percent tree cover at a spatial resolution of 500 meters: first results of the MODIS Vegetation continuous fields algorithm. Earth Interactions, 7.

Healey, S.P., Cohen, W.B., Yang, Z.Q., Krankina, O.N., 2005. Comparison of Tasseled Cap-based Landsat data structures for use in forest disturbance detection. Remote Sensing of Environment 97, 301–310.

Hilker, T., Wulder, M.A., Coops, N.C., Linke, J., McDermid, G., Masek, J.G., Gao, F., White, J.C., 2009. A new data fusion model for high spatial- and temporal-resolution mapping of forest disturbance based on Landsat and MODIS. Remote Sensing of Environment 113, 1613–1627.

Justice, C.O., Townshend, J.R.G., Vermote, E.F., Masuoka, E., Wolfe, R.E., Saleous, N., Roy, D.P., Morisette, J.T., 2002. An overview of MODIS Land data processing and product status. Remote Sensing of Environment 83, 3–15.

Key, C.H., Benson, N.C., 2005. Landscape assessment: remote sensing of severity, the normalized burn ratio. In: Lutes, D.C., et al. (Eds.), FIREMON: Fire Effects Monitoring and Inventory System. USDA Forest Service, Rocky Mountain Research Station, General Technical Report, RMRS-GTR-164-CD:LA1-LA51, Ogden, UT.

Lu, D., Mausel, P., Brondizio, E., Moran, E., 2004. Change detection techniques. International Journal of Remote Sensing 25, 2365–2407.

Luyssaert, S., Schulze, E.D., Borner, A., Knohl, A., Hessenmoller, D., Law, B.E., Ciais, P., Grace, J., 2008. Old-growth forests as global carbon sinks. Nature 455, 213–215.

Masek, J.G., Vermote, E.F., Saleous, N.E., Wolfe, R., Hall, F.G., Huemmrich, K.F., Feng, G., Kutler, J., Teng-Kui, L., 2006. A Landsat surface reflectance dataset for North America, 1990–2000. Geoscience and Remote Sensing Letters, IEEE 3, 68–72.

Masek, J.G., Huang, C.Q., Wolfe, R., Cohen, W., Hall, F., Kutler, J., Nelson, P., 2008. North American forest disturbance mapped from a decadal Landsat record. Remote Sensing of Environment 112, 2914–2926.

Pan, Y., Chen, J.M., et al., 2010. Age structure and disturbance legacy of North American forests. Biogeosciences Discussions 7 (1), 979–1020.

Roy, D.P, Boschetti, L., Trigg, S.N., 2006. Remote sensing of fire severity: assessing the performance of the normalized burn ratio. Geoscience and Remote Sensing Letters, IEEE 3, 112–116.

Ruefenacht, B., Finco, M.V., Nelson, M.D., Czaplewski, R., Helmer, E.H., Blackard, J.A., Holden, G.R., Lister, A.J., Salajanu, D., Weyermann, D., Winterberger, K., 2008. Conterminous U.S. and Alaska forest type mapping using forest inventory and analysis data. Photogrammetric Engineering & Remote Sensing 74, 1379–1388.

Song, C., Woodcock, C.E., 2003. A regional forest ecosystem carbon budget model: impacts of forest age structure and landuse history. Ecological Modelling 164, 33–47.

Tucker, C.J., Grant, D.M., Dykstra, J.D., 2004. NASA's global orthorectified landsat data set. Photogrammetric Engineering and Remote Sensing 70, 313–322.

Wimberly, M.C., Reilly, M.J., 2007. Assessment of fire severity and species diversity in the southern Appalachians using Landsat TM and ETM+ imagery. Remote Sensing of Environment 108, 189–197.

Wulder, M.A., Franklin, S.E., 2007. Understanding forest disturbance and spatial pattern: remote sensing and GIS approaches. CRC/Taylor & Francis, Boca Raton.